

Supplementary Information: Strain mapping inside an individual processed vertical nanowire transistor using scanning X-ray nanodiffraction

Dmitry Dzhigaev,^{*,†} Johannes Svensson,[‡] Abinaya Krishnaraja,[‡]
Zhongyunshen Zhu,[‡] Zhe Ren,^{†,||} Yi Liu,[†] Sebastian Kalbfleisch,[¶]
Alexander Björling,[¶] Filip Lenrick,[†] Zoltan Imre Balogh,[§]
Susanna Hammarberg,[†] Jesper Wallentin,[†] Rainer Timm,[†]
Lars-Erik Wernersson,[‡] and Anders Mikkelsen[†]

[†]*Division of Synchrotron Radiation Research and NanoLund, Department of Physics, Lund University, P.O. Box 118, SE-221 00 Lund, Sweden*

[‡]*Electrical and Information Technology, Department of Engineering, Lund University, P.O. Box 118, SE-221 00 Lund, Sweden*

[¶]*MAX IV, SE-221 00 Lund, Sweden*

[§]*DTU CEN, DTU, Fysikvej 2800, Lyngby, Denmark*

^{||}*Current address: Deutsches Elektronen-Synchrotron DESY, Notkestrasse 85, D-22607 Hamburg, Germany*

E-mail: dmitry.dzhigaev@sljus.lu.se

Sample preparation

The growth of the NWs was assisted by Au seed particles patterned in arrays by electron beam lithography on Si/InAs substrates. After annealing at 550 °C, a 150 nm long InAs segment was grown at 460 °C using trimethylindium (TMIn) and arsine (AsH₃) with a V/III ratio of 21. This is followed by a 300 nm long GaSb segment grown while heating to 515 °C using trimethylgallium (TMGa) and trimethylantimony (TMSb) with a V/III ratio of 1.26. The resulting diameters of InAs and GaSb segments were 40 nm and 70 nm respectively.

After the growth, a high-k bi-layer consisting of 1 nm Al₂O₃ and 4 nm HfO₂ was deposited using atomic layer deposition (ALD) at temperatures of 300 °C and 120 °C respectively. Next, a 30 nm W film was sputtered at an Ar pressure of 2.6 mTorr resulting in a 10 nm-thick film on the NW sidewalls. The metal on top of the NWs was then removed using a resist etchback process to define the position of the metal edge and an SF₆/Ar plasma to etch the exposed W (see Figure 1a in the main text). A low-k organic spacer (S1800) was finally used to protect and mechanically support the NWs. All these deposition and processing conditions correspond to those used for vertical MOSFET fabrication where the high-k/W is used as the gate stack. For sample protection the milled lamella was passivated with 30 nm Al₂O₃ deposited by ALD at a temperature of 100 °C.

The sample for the X-ray measurements was prepared by employing Focused Ion Beam (FIB) milling from the substrate with an array of complete devices. The major steps of the lamella preparation are shown in Figure S1. Three rows of the nanowires (NWs) were protected by Pt layer deposition on top of the organic spacer. An undercut of about 5 μm was performed by high-voltage ion beam milling, leaving a lamella of 2.5 μm thickness. After that the sample was milled from the sides until the edge rows of NWs were removed, leaving a single row of transistors within their initial environment. The lamella was glued by Pt to a micromanipulator and lifted-out for further attachment to the side of a half-moon Omniprobe grid, used as a sample holder (see Figure S1d).

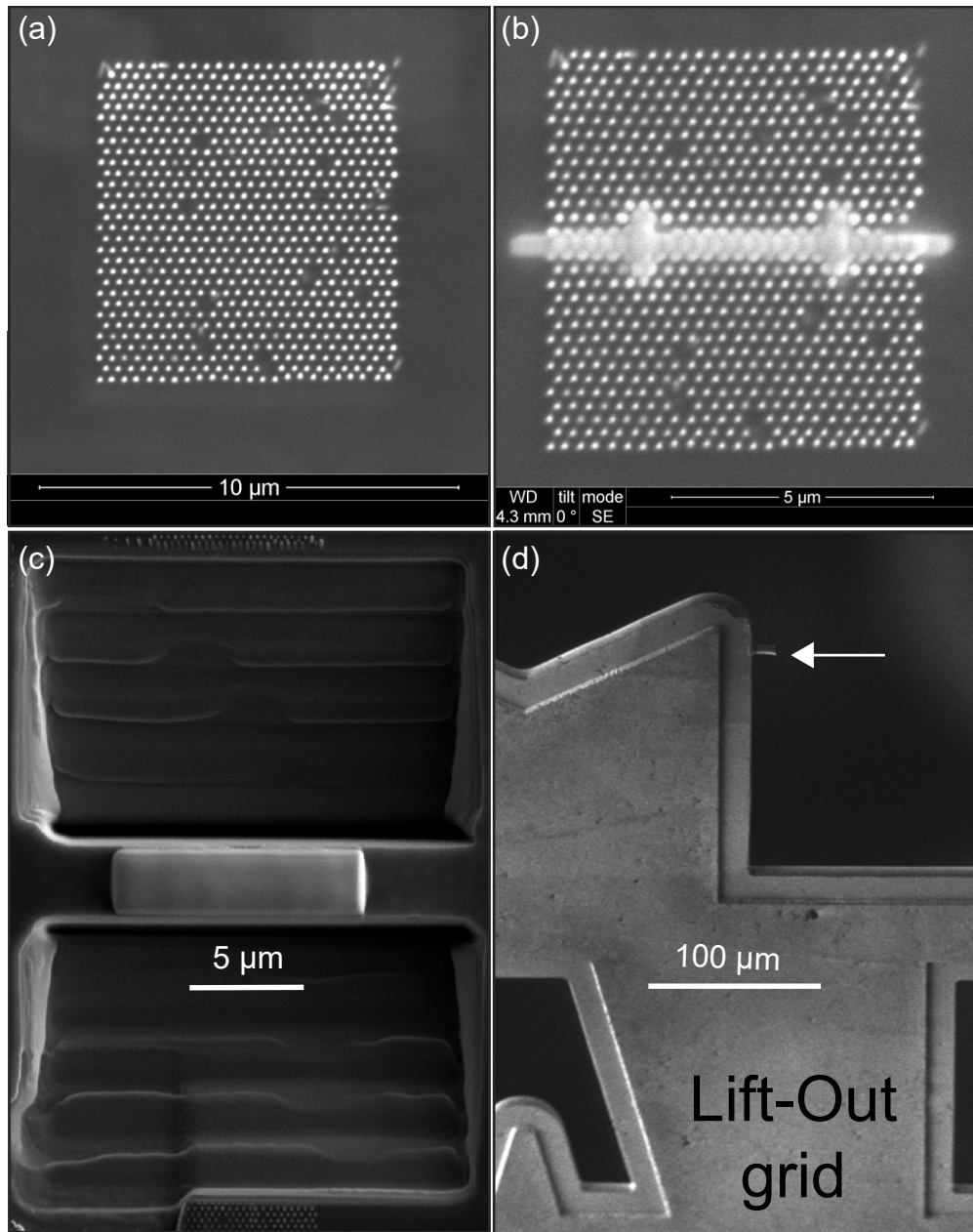


Figure S1: Scanning electron microscopy of the lamella preparation. (a) Top-view over an array of p-MOS devices covered with organic spacer. Bright dots are the positions of single NWs. (b) Deposition of Pt protective layer over 3 rows of NWs. (c) Under-cut performed by FIB milling for lamella lift-out. (d) Position of the lamella on Omniprobe Lift-Out grid by Pt "gluing".

Experimental setup and beam characterization

The sample was mounted on a goniometer of a diffractometer (Huber, Germany). The alignment and measurements of the sample were performed by in-line optical microscope,

X-ray fluorescence detector, forward scattering detector, and Bragg scattering detector mounted on the robot arm (see Figure S2).

An Xpress 3 (Quantum Detectors Ltd) X-ray fluorescence detector was located close to the sample, and perpendicular to the beam. A Pilatus 100k (Dectris) 2D hybrid pixel detector with a pixel size of $172 \times 172 \mu\text{m}^2$ was used to record far-field diffraction patterns in forward scattering 4 m downstream. A Merlin 2D detector (Quantum Detectors Ltd) with a pixel size of $55 \times 55 \mu\text{m}^2$ was positioned on a robot-arm (KUKA) providing an access to 111/0002 reflections from GaSb/InAs segments respectively.

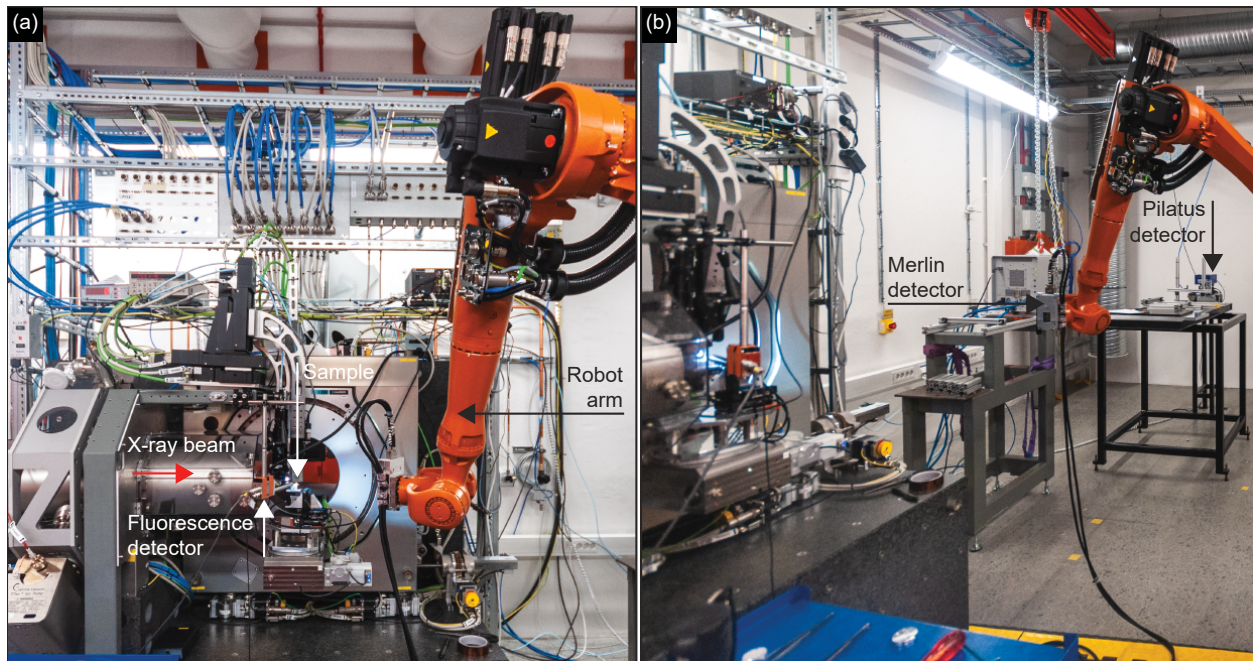


Figure S2: Photos of the experimental hutch at NanoMAX beamline (a) and (b). Corresponding detectors and elements are indicated by arrows and labels.

The beam focused by KB-mirrors was characterized by forward ptychography technique with a known test-pattern in the form of Siemens Star¹. The focal spot was optimized to have the smallest possible footprint at the sample plane (see Figure S3c) and astigmatism was minimized by evaluating the propagated wavefront (see Figure S3d). The central part of the X-ray beam shows no significant phase curvature, therefore its influence on the Bragg peak positions can be neglected.

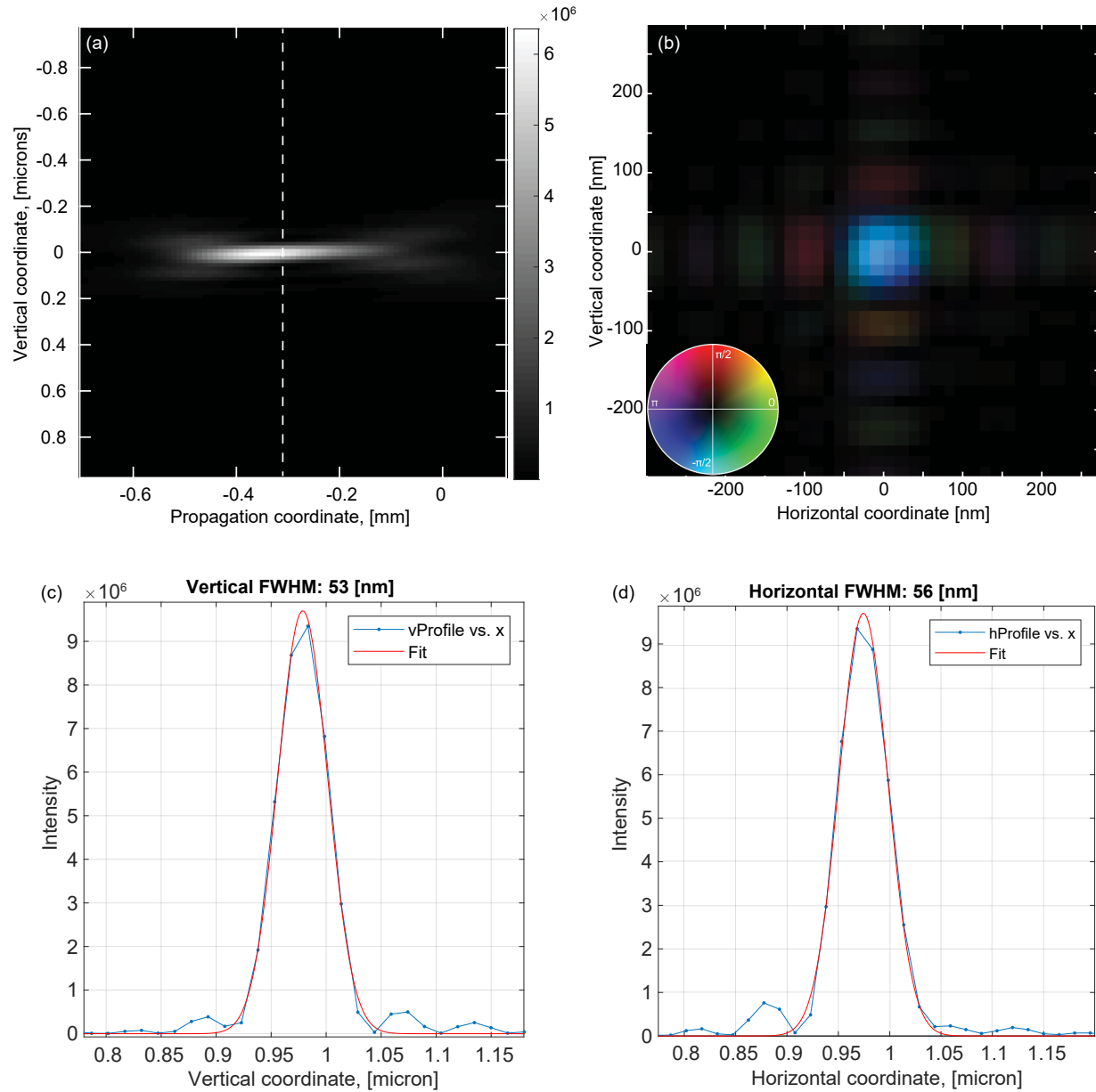


Figure S3: Ptychographic reconstruction of complex-valued X-ray beam wavefront. (a) Propagated X-ray beam profile obtained from ptychographic reconstruction. The dashed line shows the position of the sample during the experiment and is a focal plane of the beam. (b) Complex valued cross-section of the nanofocused X-ray beam at the focal plane. The phase is color coded and amplitude is brightness. Measures of FWHM of the focal spot in the vertical (c) and horizontal (d) directions.

Small angle scattering

Single NWs were located within the lamella by mapping an integrated small angle scattering intensity in the regions of interest (ROIs) as shown in Figure S4. Here, the NWs are aligned

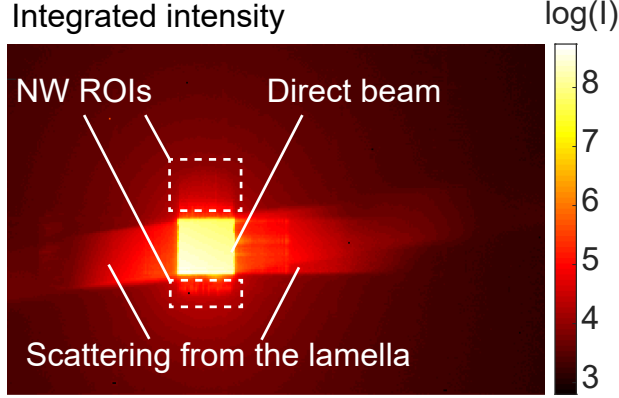


Figure S4: Small angle X-ray scattering pattern obtained by averaging the data from the lamella alignment scan recorded by Pilatus detector. The NWs are aligned along the horizontal axis. The features of the diffraction pattern are explained by the corresponding labels.

with the horizontal axis of the diffraction pattern and, therefore, produce scattering streaks in the vertical direction. They originate from the edges of the transistors, giving a perfect contrast for a single NW localization between the InAs substrate and top metal contact.

Strain and tilt calculation

The diffraction data along the rocking curve (see Figure S5a) from Merlin detector was interpolated on the orthogonal \mathbf{Q} -space coordinate system as described for example in Ref.²⁻⁴. The axis Q_x is aligned with the \mathbf{H}_{111}^{GaSb} reciprocal lattice vector. The projection of measured intensity distribution along Q_z is shown in Figure S5b, where 3 distinct Bragg peaks arise from InAs substrate, and InAs and GaSb segments. The intensity, strain, and tilt maps in the main text were calculated by evaluating the 3D center of mass (COM) of region of interest around Bragg peaks, excluding the InAs substrate peak. The strain value is obtained at each point of the scan as

$$\varepsilon = \frac{|\mathbf{Q}_0^{COM}|}{|\mathbf{Q}^{COM}|} - 1, \quad (1)$$

where \mathbf{Q}_0^{COM} is an reference COM corresponding to absence of the local strain and \mathbf{Q}^{COM} is the COM at current point of the scan. As it was discussed in the main text \mathbf{Q}_0^{COM} of the InAs Bragg peak was used as a reference for GaSb. The tilting angles around corresponding

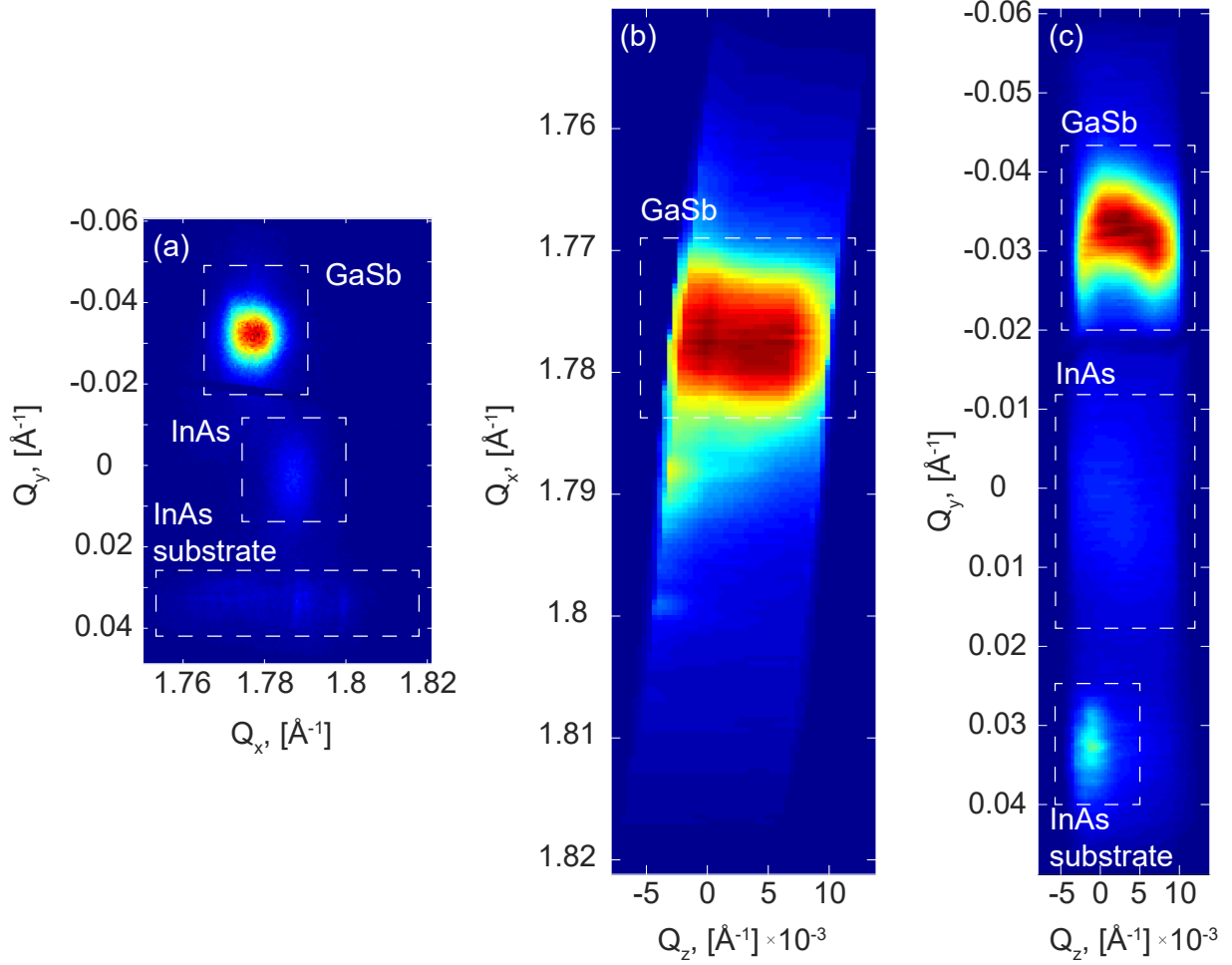


Figure S5: 2D projections of the region of reciprocal space around 111 and 0002 Bragg peaks, averaged over the whole NW. Three different regions can be distinguished here: GaSb p-type NW segment, InAs n-type NW segment, and InAs substrate. These regions were used separately to calculate the COM of peaks for each scan position in case of GaSb. The averaged Bragg peak position from InAs segment of the NW was used as a reference at each scan position.

real space axes α_z and α_y were calculated by the following expressions utilizing different

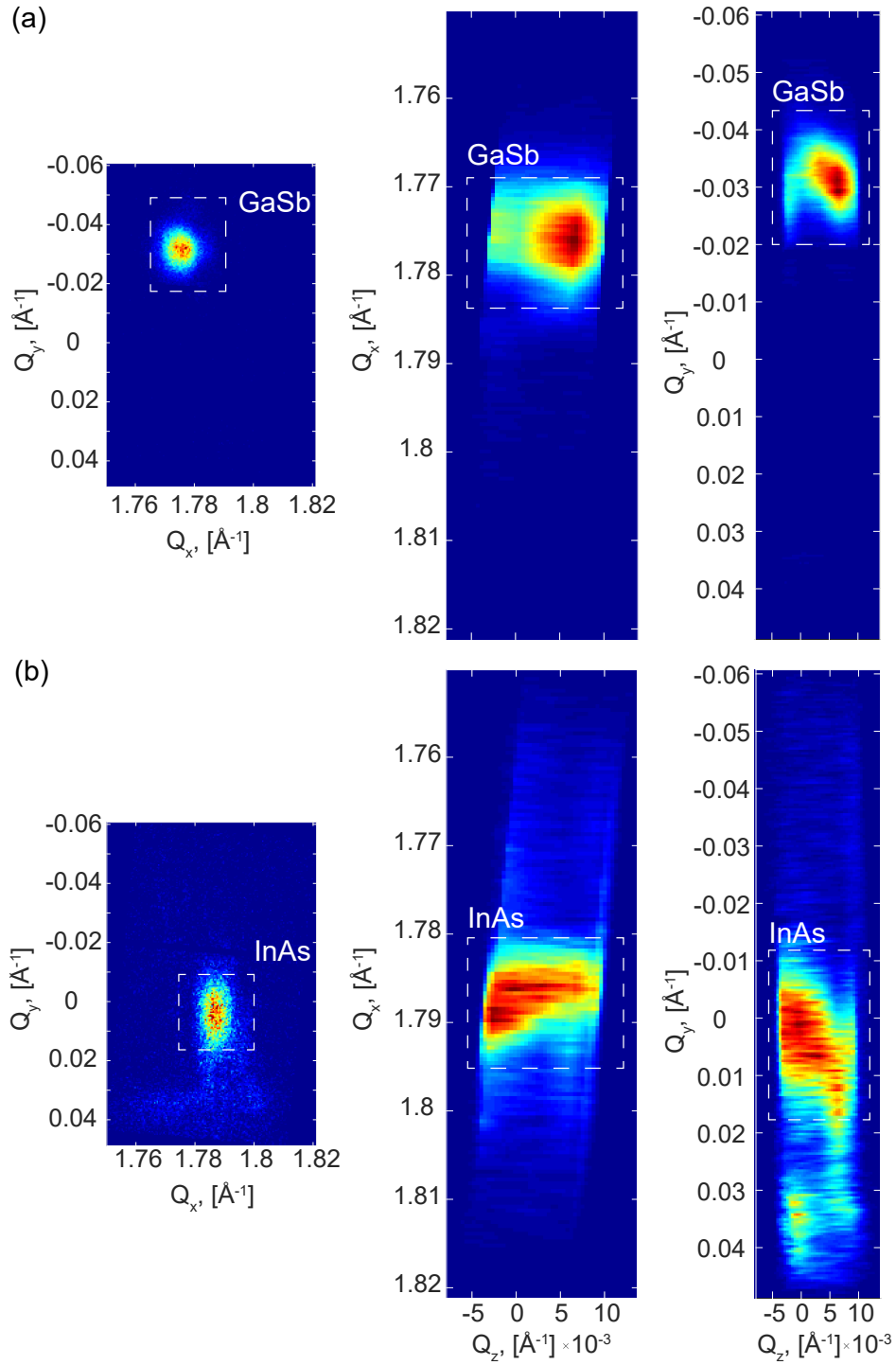


Figure S6: 2D projections of the region of reciprocal space around 111 and 0002 Bragg peaks at single scanning positions in the middle of GaSb (a) and InAs (b) segments.

Q-components of the wave-transfer vector

$$\alpha_z = \arctan\left(\frac{Q_y}{Q_x}\right), \alpha_y = \arctan\left(\frac{Q_x}{Q_z}\right). \quad (2)$$

FEM simulation

The following elastic constants were used in the FEM model^{5,6}

$$\text{InAs: } C_{11} = 8.34^{10} \text{ Pa, } C_{12} = 4.54^{10} \text{ Pa, } C_{44} = 3.95^{10} \text{ Pa}$$

$$\text{GaSb: } C_{11} = 8.83^{10} \text{ Pa, } C_{12} = 4.02^{10} \text{ Pa, } C_{44} = 4.32^{10} \text{ Pa}$$

In order to compare FEM simulation with experimental data we employed a simplified approach of averaging the strain distribution along the X-ray beam propagation direction z'

$$\langle \varepsilon_{xx}^{FEM}(x', y, z') \rangle_{z'} = \frac{1}{A(x', y)} \int \varepsilon_{xx}^{FEM}(x', y, z') dz', \quad (3)$$

here, x', y, z' is the coordinate system rotated around y-axis by Bragg angle of $\theta_B = 6.74^\circ$, $A(x', y)$ - is a cross-section of the NW along z' , and ε_{xx}^{FEM} is the FEM solution.

The experimental data in the main text was fitted by performing FEM model with varied stress induced in the W gate. The dependence of the strain state in the NW on the stress values in the W gate material is shown in Figure S7.

Bending substrate measurement

The stress in W layer can be controlled by tuning the pressure of Ar atmosphere during deposition process. An *ex situ* studies were performed on a 60 nm thick film of W deposited on a single Si (001) wafer. By measuring the bending of the wafer⁷ after W deposition the stress values were obtained (see Figure S8). The dependence was revealed to be close to linear. As it was shown in the manuscript we obtained the amount of stress induced in the W layer by employing the Finite Element Method simulation. The value of -3.1 GPa is

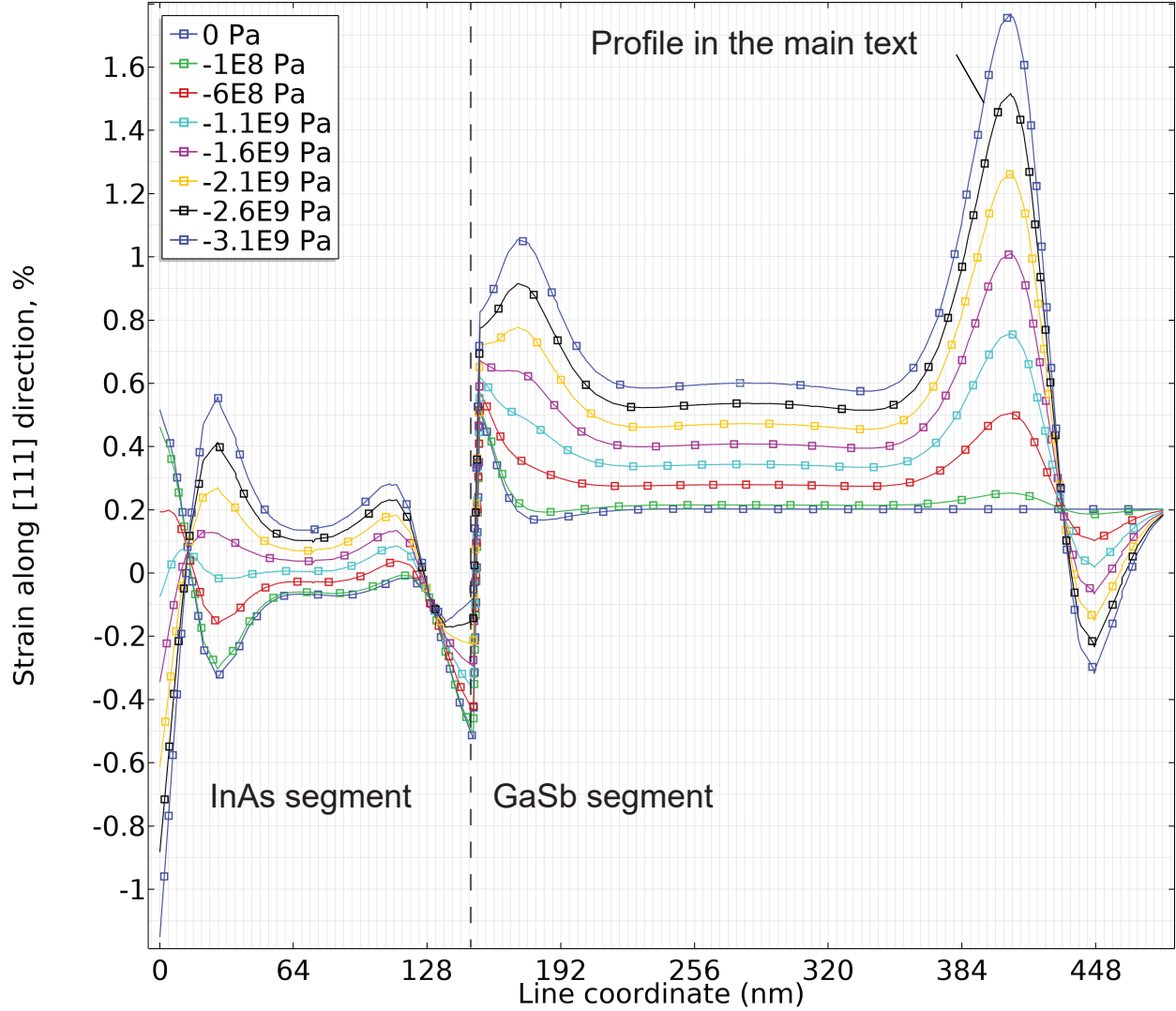


Figure S7: The profiles of the ε_{xx} strain component from the FEM simulation presented in the main text. The parameter of stress in the W gate is varied in the range from 0 to -3.1 GPa.

mapped over the plot from bending substrate measurement. Remarkably, it fits well with the Ar pressure of 2.6 mTorr which was actually used during the NW device preparation.

Beam damage

The NW sample was successfully measured thanks to short exposures and a relaxed requirement on the number of points along the rocking curve that is needed for successful diffraction

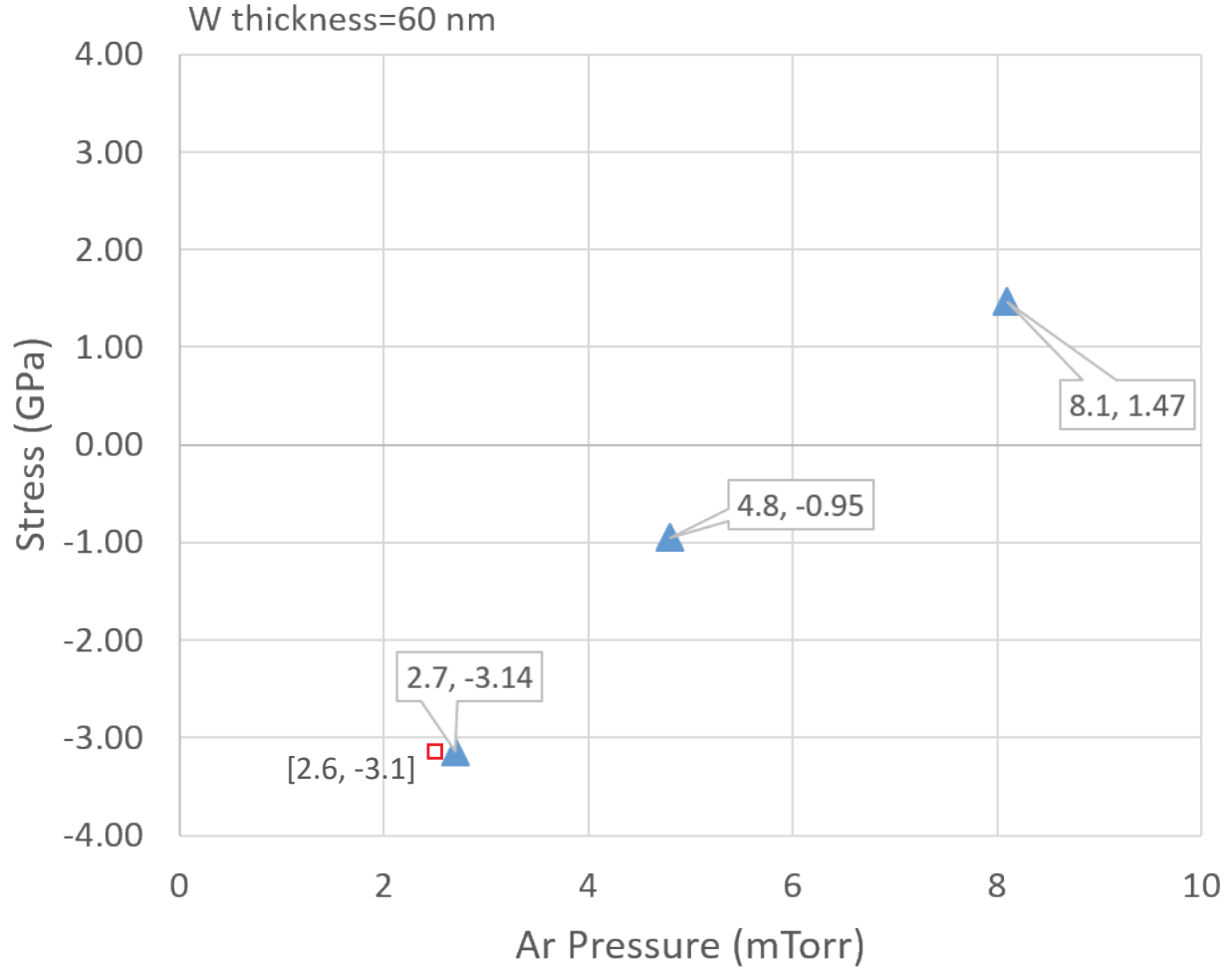


Figure S8: Dependence of stress induced in the W thin film upon deposition over Si wafer at various Ar pressure values (blue triangle markers). The stress value $\sigma_w = -3.1$ GPa obtained from the FEM simulation in the main text is mapped at 2.6 mTorr (red square marker).

mapping. However, after 5 days of intense exposure of the lamella to hard X-rays the radiation damage occurred for different layers of the lamella. The SEM images are shown in Figure S9. We believe the damaging effects include heating, surface induced deposition, and chemical instability of the low-k organic spacer between the NWs. These issues can be possibly solved by employing cryo-jet of N_2 for more effective heat dissipation and reduction of surface alternation effects. The low-k organic spacer (S1800) should be replaced by compounds more stable under intense X-ray beams.

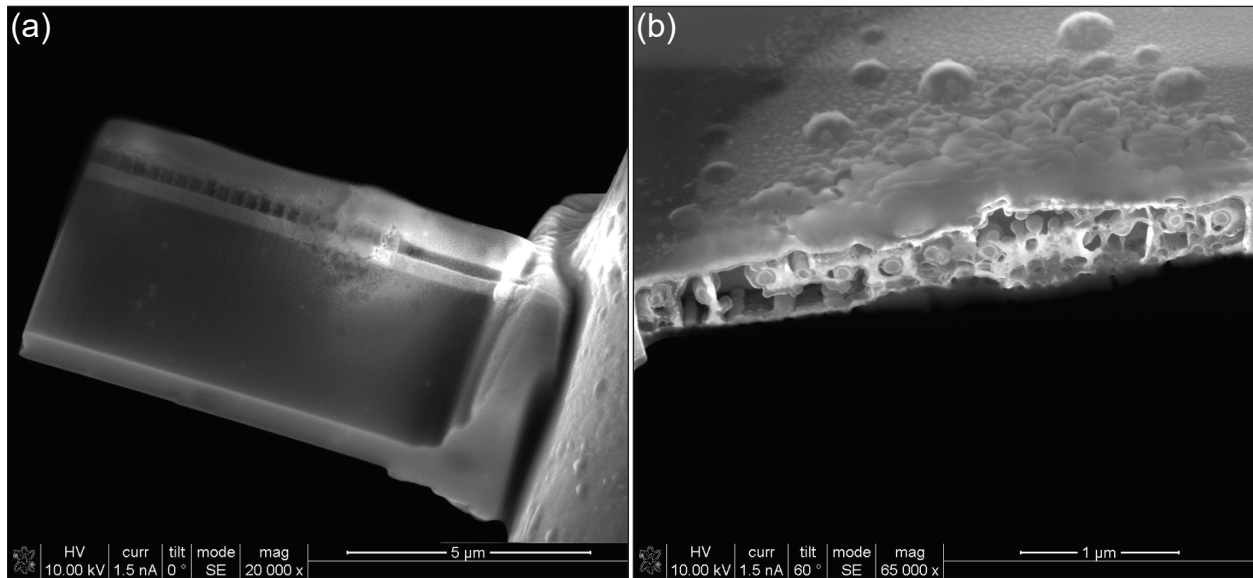


Figure S9: SEM images of the lamella damage induced by long exposure X-ray radiation. (a) A side-view over the lamella revealing surface modification. (b) A cross-sectional SEM image showing the coalescence of the spacer material. The most of the NWs can be seen in the middle of the cut.

References

1. Thibault, P.; Dierolf, M.; Bunk, O.; Menzel, A.; Pfeiffer, F. Probe Retrieval in Ptychographic Coherent Diffractive Imaging. *Ultramicroscopy* **2009**, *109*, 338 – 343.
2. Mocuta, C.; Stangl, J.; Mundboth, K.; Metzger, T.; Bauer, G.; Vartanyants, I.; Schmidbauer, M.; Boeck, T. Beyond the Ensemble Average: X-ray Microdiffraction Analysis of Single Sige Islands. *Phys. Rev. B* **2008**, *77*, 245425.
3. Stankevič, T.; Hilner, E.; Seiboth, F.; Ciechonski, R.; Vescovi, G.; Kryliouk, O.; Johansson, U.; Samuelson, L.; Wellenreuther, G.; Falkenberg, G.; Feidenhans'l, R.; Mikkelsen, A. Fast Strain Mapping of Nanowire Light-Emitting Diodes Using Nanofocused X-ray Beams. *ACS Nano* **2015**, *9*, 6978–6984.
4. Stankevič, T.; Mickevičius, S.; Schou Nielsen, M.; Kryliouk, O.; Ciechonski, R.; Vescovi, G.; Bi, Z.; Mikkelsen, A.; Samuelson, L.; Gundlach, C.; Feidenhans'l, R.

- Measurement of Strain in InGaN/GaN Nanowires and Nanopyramids. *J. Appl. Crystallogr.* **2015**, *48*, 344–349.
5. Burenkov, Y. A.; Davydov, S. Y.; Nikanorov, S. Elastic properties of indium arsenide. *Fizika Tverdogo Tela* **1975**, *17*, 2183–2186.
 6. Boyle, W. F.; Sladek, R. J. Elastic constants and lattice anharmonicity of GaSb and GaP from ultrasonic-velocity measurements between 4.2 and 300 K. *Phys. Rev. B* **1975**, *11*, 2933–2940.
 7. Schwarzer, N.; Richter, F. On the determination of film stress from substrate bending: STONEY´ s formula and its limits. **2006**,